catalysts

MDPI

Article

A New Ammonia Kinetic Model in Ru-Catalyzed Steam-Reforming Reaction Containing N_2 in Natural Gas

Chulmin Kim, Juhan Lee and Sangyong Lee *

Department of Mechanical, Robotics and Energy Engineering, Dongguk University, Seoul 04620, Republic of Korea; smkcm@naver.com (C.K.); leejuh@dgu.ac.kr (J.L.)
* Correspondence: sangyonglee@dongguk.edu

Abstract: Hydrogen for building fuel cells is primarily produced by natural-gas steam-reforming reactions. Pipeline-transported natural gas in Europe and North America used to contain about 1% to 5% N_2, which reacts with H_2 in steam-reforming reactions to form NH_3. In the case of Ru, one of the catalysts used in natural-gas steam-reforming reactions, the activity of the NH_3-formation reaction is higher than that of Ni and Rh catalysts. Reforming gas containing NH_3 is known to poison Pt catalysts in Polymer Electrolyte Membrane Fuel Cells (PEMFCs) and also poison catalysts in preferential oxidation (PROX). In this study, Langmuir–Hinshelwood-based models of the NH_3-formation reaction considering H_2 and CO were proposed and compared with a simplified form of the Temkin–Pyzhev model for NH_3-formation rate. The kinetic parameters of each model were optimized by performing multi-objective function optimization on the experimental results using a tube-type reactor and the numerical results of a plug-flow one-dimension simple SR (steam-reforming) reactor.

Keywords: hydrogen; reformation; water–gas shift reaction; kinetic model; NH_3

check for updates

Citation: Kim, C.; Lee, J.; Lee, S. A New Ammonia Kinetic Model in Ru-Catalyzed Steam-Reforming Reaction Containing N_2 in Natural Gas. *Catalysts* **2023**, *13*, 1380. https://doi.org/10.3390/catal13101380

Academic Editors: Eugenio Meloni, Marco Martino and Concetta Ruocco

Received: 2 October 2023
Revised: 16 October 2023
Accepted: 16 October 2023
Published: 19 October 2023

Copyright: © 2023 by the authors. Licensee MDPI, Basel, Switzerland. This article is an open access article distributed under the terms and conditions of the Creative Commons Attribution (CC BY) license (https://creativecommons.org/licenses/by/4.0/).

1. Introduction

Fuel-cell systems are eco-friendly power-generation systems that convert chemical energy directly into electrical energy through an electrochemical reaction, and have the potential to achieve high operating efficiencies, to produce fewer pollutants, to have flexibility in fuel sources, and to make less noise [1–3]. However, hydrogen as a fuel does not exist in nature as a pure substance, so it must be manufactured from locally available resources [4].

In general, hydrogen-production methods include reforming technologies to obtain hydrogen from fossil fuels, gasification, thermochemical methods, and water electrolysis. Hydrogen production from fossil fuels such as natural gas and petroleum-based fuels, which have long been widely used in petroleum refining and petrochemical processes, is more economical than other production methods [5]. The process of generating hydrogen through fossil-fuel reforming involves catalytic decomposition of fossil fuels in the presence of water vapor or oxygen. The reforming methods include steam reforming, partial oxidation, and auto-thermal reforming [5].

The steam-reforming method is an endothermic reaction that causes hydrocarbons to react with steam and requires a heating source in the reactor. It has the advantage of achieving high efficiency by properly controlling the heat balance in the reactor and increasing the hydrogen concentration in the product gas [5].

However, if the feed gas supplied to the reformer contains nitrogen, an ammonia-production reaction occurs as a side reaction while the methane steam-reforming (SR) reaction takes place. In fuel-cell systems, ammonia damages not only the preferential oxidation (Prox) catalyst but also the membrane of the proton-exchange membrane fuel cell (PEMFC) [6]. A study by Fumihiro Watanbe et al. showed that especially Ru catalysts among precious metal catalysts produced a significant amount of ammonia [7]. Since

Ru/Al_2O_3 is one of the most used catalysts for steam reforming, it is necessary to predict the amount of ammonia produced for PEMFC using reformers with Ru/Al_2O_3 (RUA) catalysts to prevent the damage of the Prox but also the damage of the PEMFC from ammonia. In order to predict the ammonia-formation rate that occurs simultaneously with the steam-reforming reaction in a reformer on the surface of the RUA catalyst, it is necessary to conduct NH_3-formation experiments in a steam-reforming reactor with various concentrations of N_2 containing processed natural gas as a fuel. In this research, the kinetic model based on the Langmuir–Hinshelwood mechanism by Jon Geest Jakobsen is employed for the calculation of the concentration of each gas in the steam-reforming reaction [8–10] with optimized kinetic parameters for the steam-reforming reaction on RUA catalysts. To optimize the kinetic parameters, experiments were conducted for methane steam-reforming reactions in an RUA-catalyzed tube-type reactor and the reactor surface temperature, and the compositions of the reactor outlet gas were measured via a gas analyzer (NOVA prime-MRU, Germany). To optimize kinetic parameters with experimental data, a simplified numerical model of the tube-type plug-flow packed bed reactor was implemented. For each experimental condition (reactor-feed-gas composition, reactor surface temperature, charged-catalyst amount, etc.), the outlet composition was calculated through the numerical model [11]. During the calculation of the concentration, the kinetic parameters for the model were estimated using multi-objective function optimization. For the multi-objective function optimization, MATLAB's 'fgoalattain' function was implemented, which uses the sequential-quadratic-programming (SQP) method [12]. The objective function is the result of the numerical model that calculates the exit-gas composition according to each condition. The target value is the exit composition measured in the experiment.

Various kinetic models of the ammonia-formation reaction over metal catalysts have been compared such as the Temkin–Pyzhev equation [13–17], the power law, and the Langmuir–Hinshelwood-based models. The proposed Langmuir–Hinshelwood-mechanism-based model is derived by assuming that the vacant active site in the ammonia-production reaction is occupied by carbon monoxide and/or hydrogen produced in the steam-reforming reaction [8–10]. In a new kinetic model for ammonia formation in a steam-reforming reactor, we estimated the parameters of the ammonia kinetics model with the addition of adsorption terms of carbon monoxide and/or hydrogen with experimentally obtained data.

2. Results

2.1. Numerical Modeling

2.1.1. Steam-Reforming-Reactor Model

The SR-reactor-simulation model consists of a one-dimensional model (1D model) of a tube-type reactor assuming that there is no temperature gradient in the radial direction of the reactor and the flow of the feed gas is assumed to be a plug-flow reactor. The concept of the SR-reactor-simulation model is shown in Figure 1. The numerical model of a 1D plug-flow reactor is numerically analyzed using the mass-balance, the energy-balance, and reaction-rate equations [11,18]. For the mass balance, we used the input flow rate of reactants and the reactor-outlet-gas composition measured in the experiment. The energy balance was simplified by using experimentally measured reactor surface temperature assuming that there was no temperature difference in the coaxial direction of the reactor. Therefore, the reactor numerical model in this study performs numerical analysis of the reaction kinetics of each reaction model according to the input-gas flow rate, outlet-gas composition, and reaction surface temperature at given experimental conditions.

Two major reactions in the steam-reforming (SR) reactor are considered in the SR-simulation model for a steam-reforming (SR) reaction; they are shown as Equation (1) for the steam-reforming reaction and as Equation (2) for the water–gas-shift (WGS) reaction.

$$CH_4 + H_2O \leftrightarrow CO + 3H_2 \quad (1)$$

$$CO + H_2O \leftrightarrow CO_2 + H_2 \quad (2)$$

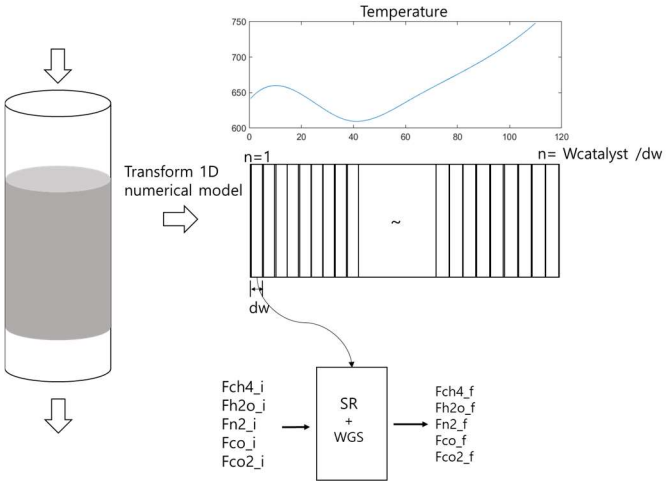

Figure 1. SR-reactor-simulation model.

To calculate the gas concentration at each location of the reactor, the one-dimensional reactor was virtually divided into N micro-cells charged with catalysts (Figure 1).

The outlet-gas composition of each micro-cell was calculated by combining the steam-reforming-reaction rate and the water–gas-shift (WGS)-reaction rate with the inlet-gas composition of the cell. The component mass-balance equations are listed as Equations (3)–(7).

$$F_{CH_4 out,n} = F_{CH_{4in,n}} - R_{SR}(T_n, P_i) \times dw \tag{3}$$

$$F_{H_2O_{out,n}} = F_{H_2O_{in,n}} - R_{SR}(T_n, P_i) \times dw - R_{WGS}(T_n, P_i) \times dw \tag{4}$$

$$F_{H_2 out,n} = F_{H_2 in,n} + 3 \times R_{SR}(T_n, P_i) \times dw + R_{WGS}(T_n, P_i) \times dw \tag{5}$$

$$F_{COout,n} = F_{COin,n} + R_{SR}(T_n, P_i) \times dw - R_{WGS}(T_n, P_i) \times dw \tag{6}$$

$$F_{CO_2 out,n} = F_{CO_2 in,n} + R_{WGS}(T_n, P_i) \times dw \tag{7}$$

$F_{iout,n}$ is the outlet molar flow rate of chemical species i in cell n and $F_{i_{in,n}}$ is the inlet molar flow rate of chemical species i in cell n. R_{SR} is the steam-reforming-reaction rate, R_{WGS} is the water–gas-shift-reaction rate, and dw is the amount of catalyst in each cell. T_n is the temperature in cell n and P_i is the partial pressure of chemical species i.

The catalytic reaction rate of the steam-reforming reaction is given as Equations (8) and (9) by Jon Geest Jakobsen [8,9].

$$R_{SR} = \frac{A_1 \cdot \exp(\frac{-E_1}{RT}) \cdot P_{CH_4} \cdot (1 - \beta_{SR})}{(1 + A_{CO} \cdot \exp(\frac{-\Delta H_{CO}}{RT}) \cdot P_{CO} + A_H \cdot \exp(\frac{-\Delta H_H}{RT}) \cdot P_{H_2}^{\frac{1}{2}})^2} \tag{8}$$

$$\beta_{SR} = \frac{P_{CO} P_{H_2}^3}{P_{CH_4} P_{H_2O}} \cdot \frac{1}{K_{P,SR}} \tag{9}$$

$$K_{P,SR} = SR_{equilibrium}(FCH_{4in,n}, FH_2O_{in,n}, FH_{2in,n}, FCO_{in,n}, FCO_{2in,n}) \tag{10}$$

A_1 is the Arrhenius constant and E_1 is the activation energy. A_{co} and A_H are the prefactors of the CO and H equilibrium constants, and ΔH_{CO} and ΔH_H are the enthalpies of adsorption. β_{SR} is the approach to the SR-reaction equilibrium [8] and P_i is the partial pressure of chemical species i. $K_{P,SR}$ is the thermodynamic equilibrium constant of the SR reaction.

The water–gas-shift reaction was calculated using the WGS kinetics model by Jian Sun as shown in Equations (11)–(13) [19].

$$R_{WGS} = \frac{A \cdot \exp\left(\frac{-E}{RT}\right) \cdot P_{CO} P_{H_2O} \cdot (1 - \beta_{WGS})}{\left(1 + A_{CO} \cdot \exp\left(\frac{-\Delta H_{CO}}{RT}\right) \cdot P_{CO}\right) \cdot \left(1 + A_{H_2} \cdot \exp\left(\frac{-\Delta H_{H2}}{RT}\right) \cdot P_{H_2}\right)} \quad (11)$$

$$\beta_{WGS} = \frac{P_{CO_2} P_{H_2}}{P_{CO} P_{H_2O}} \cdot \frac{1}{K_{P,WGS}} \quad (12)$$

$$K_{P,WGS} = WGS_{equilibrium}\left(FCH_{4in,n}, FH_2O_{in,n}, FH_{2in,n}, FCO_{in,n}, FCO_{2in,n}\right) \quad (13)$$

A is the Arrhenius constant and E is the activation energy in the WGS reaction. A_{co} and A_{H2} are the prefactor of the CO and H equilibrium constants, and ΔH_{CO} and ΔH_{H2} are the enthalpies of adsorption. B_{WGS} is the approach to the WGS-reaction equilibrium and P_i is the partial pressure of chemical species i. $K_{P,WGS}$ is the thermodynamic equilibrium constant of the WGS reaction.

The initial values of the kinetics parameter of the reactor numerical model for the SR reaction and WGS reaction in experimental setup 1 (Section 3) are summarized in Table 1 [8,19].

Table 1. Initial values of the kinetic model for SR-reactor simulation [8,19].

Steam-Reforming Kinetics Parameters					
A_1 (mol/g·h·bar)	E_1 (kJ/mol)	A_{co} (bar^{-1})	ΔH_{co} (kJ/mol)	A_H ($bar^{-1/2}$)	ΔH_H (kJ/mol)
4.39×10^7	107.9	2.19×10^{-5}	−87.4	7.31×10^{-6}	−71
Water–Gas-Shift Kinetics Parameters					
A ($mol/m^3.atm^2.s$)	E (kJ/mol)	A_{co} (atm^{-1})	ΔH_{co} (kJ/mol)	A_{H2} (atm^{-1})	ΔH_{H2} (kJ/mol)
2.00×10^7	43	9.40×10^{-11}	−100	1.10×10^{-10}	−90

2.1.2. Ammonia-Formation Kinetic Model in the SR Reactor

Two models were applied and compared for the prediction of the ammonia-formation rate in the SR reactor where a small amount of nitrogen is supplied to the SR reactor with methane. The most commonly used rate equation for ammonia synthesis is the Temkin–Pyzhev equation, proposed in 1940, which is derived by assuming that dissociative adsorption of nitrogen determines the rate and catalyst surface occupancy by nitrogen atoms is high [17]. Ozaki et al. proposed a rate equation (Equation (14)) that extends the original Temkin–Pyzhev equation when the surface occupancy of atomic nitrogen is not high [14,16]. In this study, the Temkin–Pyzhev equation extended by Ozaki (Equation (14)) was simplified to a power-law model as shown in Equations (15)–(18), assuming that there is an excess of hydrogen relative to ammonia in the reactor due to the high conversion of methane at the steam-reforming reaction [13,14,16,17]. Then, the calculation result was compared with a newly derived model.

$$R_{NH_3} = \frac{k'_A P_{N_2} - k'_B \left(P_{NH_3}\right)^2 / \left(P_{H_2}\right)^3}{\left[1 + k'_B \left(P_{NH_3}\right) / \left(P_{H_2}\right)^{3/2}\right]^{2\alpha}} \quad (14)$$

$$\text{If } P_{H_2} \gg P_{NH_3} \rightarrow k'_B \left(P_{NH_3}\right)^2 / \left(P_{H_2}\right)^3 \approx 0, \left[1 + k'_B \left(P_{NH_3}\right) / \left(P_{H_2}\right)^{\frac{3}{2}}\right]^{2\alpha} \approx 1 \quad (15)$$

$$R_{NH_3} = \frac{k'_A P_{N_2} - k'_B (P_{NH_3})^2 / (P_{H_2})^3}{\left[1 + k'_B (P_{NH_3}) / (P_{H_2})^{3/2}\right]^{2\alpha}} \cong k_{NH_3} \cdot P_{N_2} \quad (16)$$

$$R_{NH_3} = k_{NH_3} \cdot P_{N_2} \quad (17)$$

$$k_{NH_3} = A_{n2} \cdot \exp\left(\frac{-E_{n2}}{RT}\right) \quad (18)$$

Since the dominant reaction affecting the concentration of each component is the steam-reforming reaction and the WGS reaction, although these reactions proceed simultaneously with the ammonia-formation reaction inside the methane-steam-reforming reactor, the concentration of each component including hydrogen in a micro-cell in Figure 1 is calculated using Equations (8) and (11). The kinetics of the steam-reforming reaction over Ru/ZrO_2 catalysts by J.G. Jakobsen et al. [8] showed that CO and H atoms partially cover the catalyst surface at low temperatures, reducing the methane-steam-reforming activity [8,9]. Thus, the assumption that hydrogen and CO occupy the active sites on the catalyst with dissociative adsorption of nitrogen as the rate-determining step is applied for a new Langmuir–Hinshelwood-type kinetic model for ammonia formation in the SR reactor. The new kinetic model is explained in Equations (19)–(24) [8–10].

$$R_{NH_3} = k_{NH_3} P_{N_2} {\theta_v}^2 \quad (19)$$

$$\theta_v = (1 - \theta_N - \theta_{CO} - \theta_H) \quad (20)$$

$$K_{CO} = A_{CO} \cdot \exp\left(\frac{-\Delta H_{CO}}{RT}\right) \quad (21)$$

$$K_H = A_H \cdot \exp\left(\frac{-\Delta H_H}{RT}\right) \quad (22)$$

$$R_{NH_3} = \frac{k_{NH_3} P_{N_2} \cdot (1 - \beta_{NH_3})}{\left(1 + K_{CO} P_{CO} + K_H {P_{H_2}}^{1/2}\right)^2} \quad (23)$$

$$R_{NH_3} = \frac{k_{NH_3} P_{N_2} \cdot (1 - \beta_{NH_3})}{(1 + K_{CO} P_{CO})^2} \quad (24)$$

$$R_{NH_3} = \frac{k_{NH_3} P_{N_2} \cdot (1 - \beta_{NH_3})}{\left(1 + K_H {P_{H_2}}^{1/2}\right)^2} \quad (25)$$

A_{n2} is the Arrhenius constant and E_{n2} is the activation energy in ammonia-formation reactions. A_{co} and A_H are the prefactor of the CO and H equilibrium constants, and ΔH_{CO} and ΔH_H are the enthalpies of adsorption. β_{NH3} is the approach to the ammonia-formation-reaction equilibrium, and P_i is the partial pressure of chemical species i. $K_{P,WGS}$ is the thermodynamic equilibrium constant of the WGS reaction. θ_i is the active site on the catalyst surface of chemical species i.

The initial parameters of the power-law model for ammonia kinetics (Equation (16)) during parameter optimization using preliminary experimental data obtained in this study are summarized in Table 2.

Table 2. Initial parameters of the power-law model for NH_3 formation [20].

NH_3 Kinetics Parameters	
A_1 (mol/g·h·bar)	**E_1 (kJ/mol)**
5	80

2.1.3. Numerical Models for Estimating Kinetic Parameters

The process block diagram for optimizing the kinetic parameters of the SR reaction, the kinetic parameters of the WGS reaction, and of the kinetic parameters of the NH_3-formation reaction using the measured reactor temperatures and outlet-gas compositions in experiment set 1 (Section 3) and in experiment set 2 (Section 3) is shown in Figure 2.

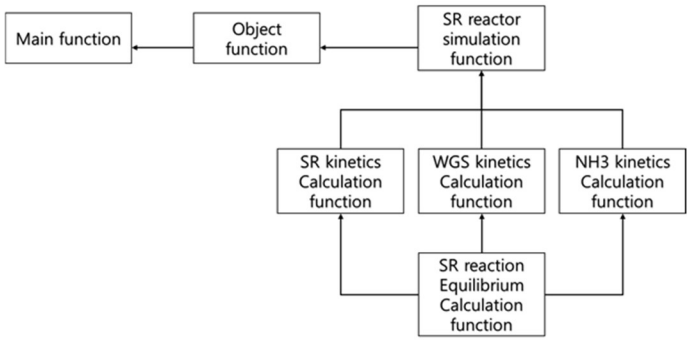

Figure 2. Process diagram for kinetic-parameter optimization.

The main function is to optimize the kinetics parameters of each reaction using MATLAB's multi-objective optimization function 'fgoalattain', which starts from the initial value of the kinetics parameters of the chemical reaction and optimizes the kinetic parameters to reduce the difference between the experimentally measured reactor-outlet-gas compositions at each experimental condition. The resulting value (objective value) is the calculated concentration of outlet flow, which is calculated via the objective function with adjusted kinetic parameters for the optimization process. The main function is made up of Equations (26)–(31).

Optimization variable

$$X = \left[SR_{parameters}, WGS_{parameters}, NH_{3.parameters}\right] \quad (26)$$

Kinetic parameters

$$SR_{parameters} = [A_1\ E_1\ A_{CO}\ \Delta H_{CO}\ A_H\ \Delta H_H] \quad (27)$$

$$WGS_{parameters} = \left[A\ E\ A_{CO}\ \Delta H_{CO}\ A_{H_2}\ \Delta H_{H_2}\right] \quad (28)$$

$$NH_{3.parameters} = [A_{n2}\ E_{n2}] \quad (29)$$

The kinetic parameters of each reaction are those of the SR-reaction kinetic Equation (8), the WGS-reaction kinetic Equation (11), and the NH_3-reaction kinetic Equation (18).

The constant is each experiment's conditions.

$$C_j = \left[f_{input}, T_{surface}, x_{catalyst}\right] \quad (30)$$

j is the experiment number and C_j is the conditions for each experiment. f_{input} is input flow rate, $T_{surface}$ is the temperature profile on the reactor surface, and $x_{catalyst}$ is the catalyst weight distribution based on location in the reactor.

Multi-objective optimization function

$$X_{optimal} = \text{fgoalattain}\left(F_{object}, X_{initial}, \text{goal}, \text{weight.etc}\right) \quad (31)$$

$X_{optimal}$ is the result of the optimized variable. $X_{initial}$ is the initial value of the optimization variable. Goal is the target value (experimental data). F_{object} is the objective function. The objective function is generated as shown in Equation (32) in the objective-function block using the results of Equation (33), the SR-reactor numerical model.

The objective function runs the SR-reactor-simulation function with the kinetic parameters from the main function as variables and the reactant input flow rate and reactor surface temperature as constants for each experimental condition. The reactor-outlet-composition value, which is the calculation result of the SR-reactor-simulation function for each experimental condition, is returned to the objective function as a matrix for comparison with the objective value of the main function.

Objective function

$$F_{objet} = \begin{bmatrix} F_{SR}(X, C_1)_1 \\ \vdots \\ F_{SR}(X, C_n)_n \end{bmatrix} \quad (32)$$

SR-reactor numerical function

$$\left[F_{CH_4}\ F_{H_2O}\ F_{H_2}\ F_{CO}\ F_{CO_2}\ F_{N_2}\ F_{NH_3}\right] = F_{SR}\left(X, C_j\right)_j \quad (33)$$

$F_{SR}()_j$ is the SR-reactor-numerical-model function at the jth experimental condition.

The SR-reactor-simulation function consists of the SR-kinetics function, the WGS-kinetics function, the NH_3-kinetics function, and the equilibrium-calculation function that uses Gibb's minimization to calculate the equilibrium concentration for a given gas concentration and temperature. This function divides the total amount of catalyst in the reactor by the amount of micro-catalyst, dw, to make n calculation cells, as shown in the conceptual diagram in Figure 1. Each cell calculates the degree of reaction of each reactant and passes it to the next cell by calling the function named kinetics of each reaction with the temperature of the cell as an input variable in addition to the flow rate and concentration of the input gas from the previous cell. The calculation of each cell is performed sequentially, and the calculated concentration of the last nth cell is the outlet concentration of the reactor. The SR-reaction kinetics and the WGS-reaction kinetics for the SR-reactor simulation used the kinetics parameters estimated with the experimental data in experiment set 1. The kinetics parameters of the ammonia-production reaction were estimated via multi-objective function optimization in MATLAB using the SR-reactor numerical model as the objective function, with the measured gas-composition values at the reactor outlet in experiment set 2 as the objective values.

3. Experimental Results

3.1. Steam-Reforming and Water-Gas-Shift Reactions

3.1.1. Experimental Results

Experiment set 1 was performed to optimize the kinetic parameters of the Ru-catalyzed steam-reforming (SR) reaction and water–gas-shift (WGS) reaction. In the experiments, the surface temperature of the tube-type reactor was measured after the reaction reached a steady state as shown in Table 3.

The dry base composition after removing water from the reactor outlet gas for each experimental condition is summarized in Table 4.

Table 3. Reactor-surface-temperature measurements from experiment set 1.

Reactor-Surface-Temperature Measurements						
Experiment No.	**TC1**	**TC2**	**TC3**	**TC4**	**TC5**	**TC6**
1	416.103	427.890	490.712	541.452	614.178	688.963
2	421.888	428.360	488.376	537.954	610.327	686.980
3	402.377	439.223	508.940	561.301	637.521	715.646
4	403.623	436.523	504.549	554.959	627.075	705.193
5	427.960	469.278	535.604	591.280	675.579	761.531
6	432.481	453.047	530.301	586.076	665.849	757.463
7	444.038	487.878	560.254	621.675	723.599	824.274
8	453.183	470.034	555.041	613.283	708.914	819.654

Table 4. SR-reactor-outlet-composition measurements from experiment set 1.

Measured Composition of the Reactor Outlet Gas (Dry Base)							
Experiment No.	**Furnace Setup Temp.**	**F_{CH4} (mol/)**	**CH_4 (%)**	**H_2 (%)**	**CO (%)**	**CO_2 (%)**	**CH_4 Conversion (%)**
1	500	2.6771	6.4341	71.7208	11.9954	11.0434	78.18
2	500	2.9449	6.8156	71.5951	11.1548	11.5788	76.92
3	520	2.6771	4.2164	73.0609	14.2023	9.8340	85.06
4	520	3.4803	5.2540	72.6521	11.8964	11.3181	81.56
5	550	2.6771	2.0439	74.2690	17.4827	7.8603	92.55
6	550	3.4803	2.1483	74.6066	15.0817	9.6202	91.99
7	580	2.6771	0.3226	75.3647	19.4244	6.8561	98.80
8	580	3.7480	0.4790	75.6000	17.4718	8.2331	98.17

3.1.2. Calculation Results

A 1D plug-flow reactor model was applied to optimize the kinetic parameters of Equation (8) for the SR-reaction rate and the kinetic parameters of Equation (11) for the WGS-reaction rate. To optimize the kinetic parameters, the calculated composition of the outlet gas and the measured composition of the outlet gas were compared to minimize the difference. The optimized kinetic parameters are summarized in Table 5. A comparison between the calculated concentration of each gas in the outlet gas and the measured concentration of it in experiment set 1 is summarized in Figure 3.

Table 5. Estimated SR-reaction and WGS-reaction kinetic parameters.

Steam-Reforming Kinetics Parameters					
A_1 (mol/g.h.bar)	E_1 (kJ/mol)	A_{co} (bar^{-1})	ΔH_{co} (kJ/mol)	A_H ($bar^{-1/2}$)	ΔH_H (kJ/mol)
4.3785×10^7	1.2768×10^2	9.0900×10^{-5}	-9.5343×10^1	6.7500×10^{-6}	-7.6548×10^1
WGS Kinetics Parameters					
A ($mol/m^3.atm^2.s$)	E (kJ/mol)	A_{co} (atm^{-1})	ΔH_{co} (kJ/mol)	A_{H2} (atm^{-1})	ΔH_{H2} (kJ/mol)
1.9991×10^7	4.2383×10^1	3.6400×10^{-11}	-9.9403×10^1	3.6000×10^{-11}	-8.8443×10^1

The graph in Figure 3 displays the measured values from experiment set 1 on the *x*-axis and the calculated values from the numerical model on the *y*-axis. As shown in Figure 3, the kinetic model with optimized parameters can predict most gas concentrations within a 20% error, except methane, hydrogen, and CO_2. For hydrogen and CO_2, the model can predict each concentration within a 5% error. In the case of methane-concentration prediction, the prediction error is less than 10% in the low-conversion region. As methane conversion increased from low to high levels, methane concentrations were under-predicted, resulting in an average error of 42.64% (Table 6).

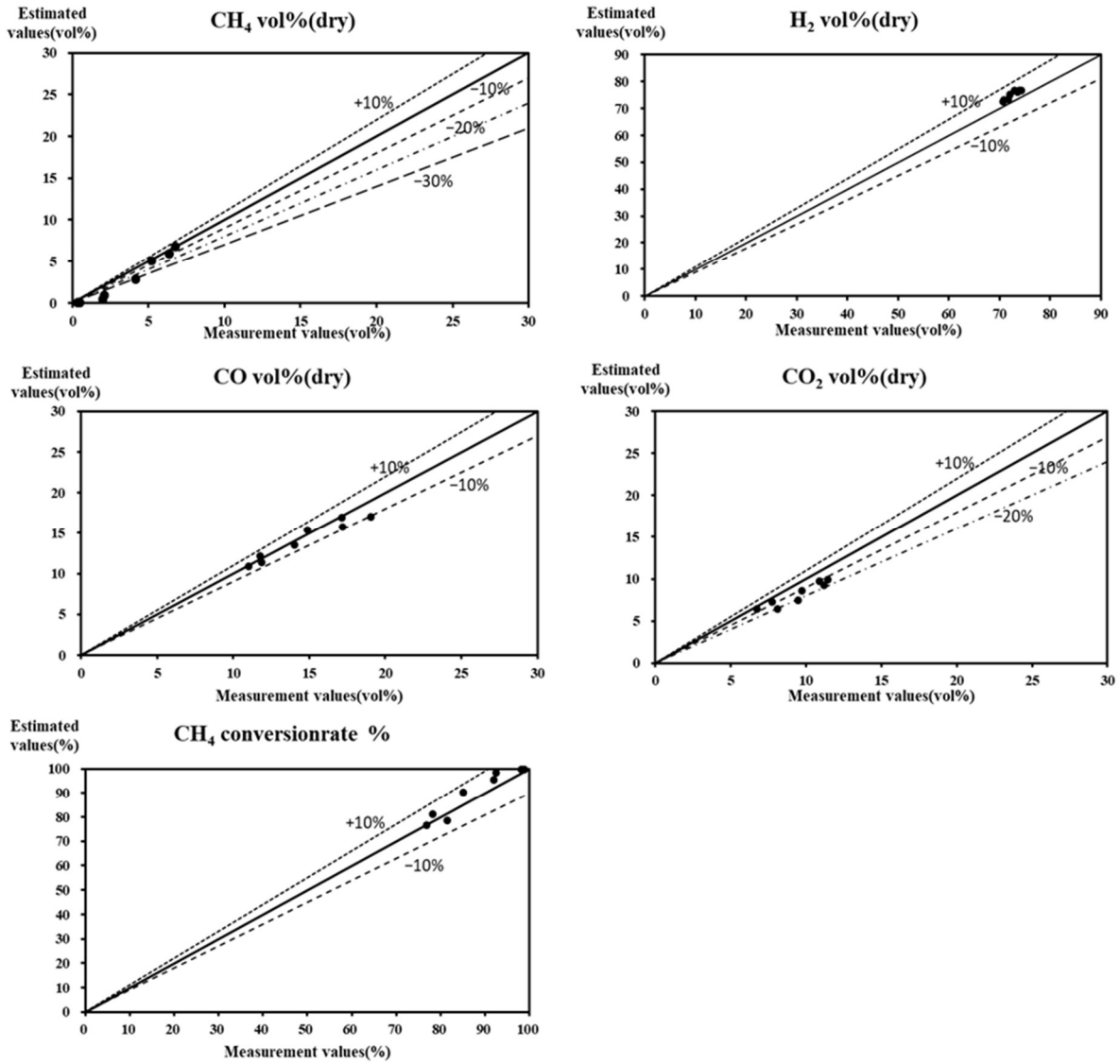

Figure 3. SR- and WGS-reaction-simulation results vs. experiment results in Table 4. Black circle (●) indicate measured and calculated values under the same experimental conditions.

Table 6. SR- and WGS-reaction-simulation results vs. experiment results average errors.

Average Error (%)				
CH_4	H_2	CO	CO_2	CH_4 Conversion Rate
42.64	3.32	4.46	13.16	3.31

3.2. NH_3 Formation Reaction

3.2.1. Experimental Results

The temperature-measurement scheme is shown in Section 4 Experiments, and the measured temperature values are shown in Table 7. TC1 is the topmost part of the reactor surface of the catalyst bed where the gas flows in, and TC3 measures the surface temperature of the bottommost part of the catalyst bed in the reactor.

Table 7. Reactor-surface-temperature-measurement results from experiment set 2.

Reactor-Surface-Temperature Measurements			
Experiment No.	**TC1**	**TC2**	**TC3**
1	434.2252	553.9525	595.2163
2	458.5575	586.2754	632.4215
3	483.6517	619.8598	672.3031
4	499.0160	644.0106	700.7845
5	513.5956	668.8458	731.3515
6	530.3918	710.7519	789.1044
7	548.0571	755.8316	834.4375
8	440.0291	556.2471	605.9996
9	463.8518	588.7224	646.0989
10	487.6856	622.2952	686.5030
11	501.8929	645.3193	713.8137
12	516.5297	670.3384	747.8994
13	537.5016	712.1737	798.3009
14	548.4273	744.9738	830.3618
15	437.2601	560.6386	610.6106
16	462.3212	593.1973	644.3216
17	486.0982	629.5613	679.6483
18	504.6832	652.3975	713.9694
19	518.6271	675.0642	736.6576
20	541.1640	714.3720	786.7085
21	553.4275	741.6453	815.8044
22	443.5432	560.9095	602.7401
23	470.3663	593.2220	644.9947
24	496.1722	625.3554	687.1435
25	513.8378	641.2851	711.8383
26	528.0075	663.2032	746.5344
27	540.0961	702.7927	810.3330

The composition of the reactor outlet gas in experiment set 2 was measured in a gas analyzer (NOVA prime, MRU) after the water vapor contained in the outlet gas was removed from the cooler. Ammonia concentration was determined by condensing the outlet gas in a cooler for 20 to 30 min and measuring the ammonia dissolved in the condensate using colorimetric determination. The total molar flow rate was calculated using the volumetric composition of the dry gas measured on the gas analyzer for the outlet gas while the condensate was collected over a period of time. The ammonia flow rate was calculated by adding the amount of ammonia in the condensate and exhaust gases. The results of measuring the outlet-gas concentrations of the SR reactor are listed in Table 8.

Table 8. Reactor-outlet-composition measurements from experiment set 2.

Reactor-Outlet-Composition Measurement								
Experiment No.	**Furnace Setup Temp.**	**F_{CH4} (mol/h)**	**CH_4 (%)**	**H_2 (%)**	**CO (%)**	**CO_2 (%)**	**NH_3 (ppm)**	**CH_4 Conversion (%)**
1	520	2.8295	11.4679	69.6571	5.8750	12.5571	2.1949	61.65
2	550	2.7278	7.5450	72.8300	8.3900	11.3350	3.8545	72.32
3	580	2.6314	4.3583	75.4958	11.3250	9.8083	6.9101	82.90
4	600	2.5725	2.7750	76.5813	13.1533	8.6125	10.4133	88.67
5	620	2.5136	1.4444	77.4389	14.7889	7.4667	13.9303	93.92
6	650	2.4333	0.3067	78.1733	16.2533	6.5000	15.2267	98.66
7	680	2.3557	0.0765	78.3412	16.5706	6.2882	11.7188	99.65
8	520	2.8054	12.8150	68.4650	5.8350	12.4400	2.6023	58.78
9	550	2.7037	8.2000	72.0348	8.4957	11.1565	4.2844	70.57
10	580	2.6100	5.2609	74.0696	11.5348	9.2435	8.7123	79.79

Table 8. *Cont.*

Reactor-Outlet-Composition Measurement								
Experiment No.	**Furnace Setup Temp.**	**F_{CH4} (mol/h)**	**CH_4 (%)**	**H_2 (%)**	**CO (%)**	**CO_2 (%)**	**NH_3 (ppm)**	**CH_4 Conversion (%)**
11	600	2.5484	3.0895	75.7000	13.2316	8.2421	13.2180	87.42
12	620	2.4922	1.2292	75.7125	14.6250	7.4583	17.9330	94.73
13	650	2.4119	0.2040	76.5120	15.6320	6.8480	19.3508	99.12
14	670	2.3610	0.0600	76.6500	15.7000	6.8100	17.4777	99.73
15	520	2.7840	11.9455	67.3864	5.7591	12.4364	3.3526	60.36
16	550	2.6823	7.3000	70.8850	8.3000	11.2950	5.8103	72.86
17	580	2.5859	4.7913	72.6261	11.5261	9.1565	11.9798	81.20
18	600	2.5297	2.6565	74.2217	13.2696	8.2130	20.2724	88.98
19	620	2.4708	1.2875	75.2292	14.7167	7.2375	25.2017	94.45
20	650	2.3905	0.2760	75.9200	15.8720	6.4920	26.0380	98.76
21	670	2.3396	0.1040	76.0000	16.2080	6.2480	20.4790	99.56
22	520	2.6769	12.4650	66.0600	5.4950	12.1950	4.2351	58.67
23	550	2.6769	7.5909	70.2682	8.0045	11.2500	8.4266	71.72
24	580	2.6769	4.2409	72.8091	10.6273	9.8136	13.4893	82.82
25	600	2.6769	2.1500	74.3727	12.1773	8.9455	19.1980	90.76
26	620	2.6769	0.9952	75.1143	13.5476	8.0381	25.0476	95.57
27	650	2.6769	0.3043	75.6130	15.3304	6.8522	21.5246	98.67

3.2.2. Comparison between Calculated Values and Measured Valued

The formation rate of NH_3 was calculated via two kinetic models and the calculation results were compared with experimental data. The first model is the power-law model, and the second model is the newly derived kinetic model based on the Langmuir–Hinshelwood mechanism. The power-law model is given as Equations (14)–(17) and the optimized kinetic parameters in Equation (17) are in Table 9. The concentration of NH_3 in the outlet gas was calculated via the power-law model and compared with experimental data in experiment set 2; this is summarized in Figure 4. As mentioned, the concentrations of the remaining components are calculated with Equations (8) and (11).

Table 9. NH_3 power-law parameters results.

NH_3 Kinetics Parameters Results	
A_{n2} (mol/g.h.bar)	**E_{n2} (kJ/mol)**
4.9809	8.0787×10^1

The NH_3 concentration of SR-reactor outlet gas was calculated via the power-law model and compared with experimental data obtained in experiment set 2. Then, the concentration of NH_3 was calculated via the newly derived Langmuir–Hinshelwood-mechanism-based kinetic model and compared with experimental data. For the calculation of the rest of the species, Equation (8) by Geest Jakobsen for the SR-reaction rate [8,10] and Equation (11) by Jian Sun for the WGS-reaction rate [19] were employed. The optimized kinetic parameters for the power-law model are listed in Table 9, the average error for power-law model are listed in Table 10 and those for the new kinetic model are in Tables 11–14.

Table 10. Average errors in Figure 4 results.

Average Error (%)					
CH_4	**H_2**	**CO**	**CO_2**	**NH_3**	**CH_4 Conversion Rate**
43.99%	4.28%	8.84%	3.92%	88.29%	8.53%

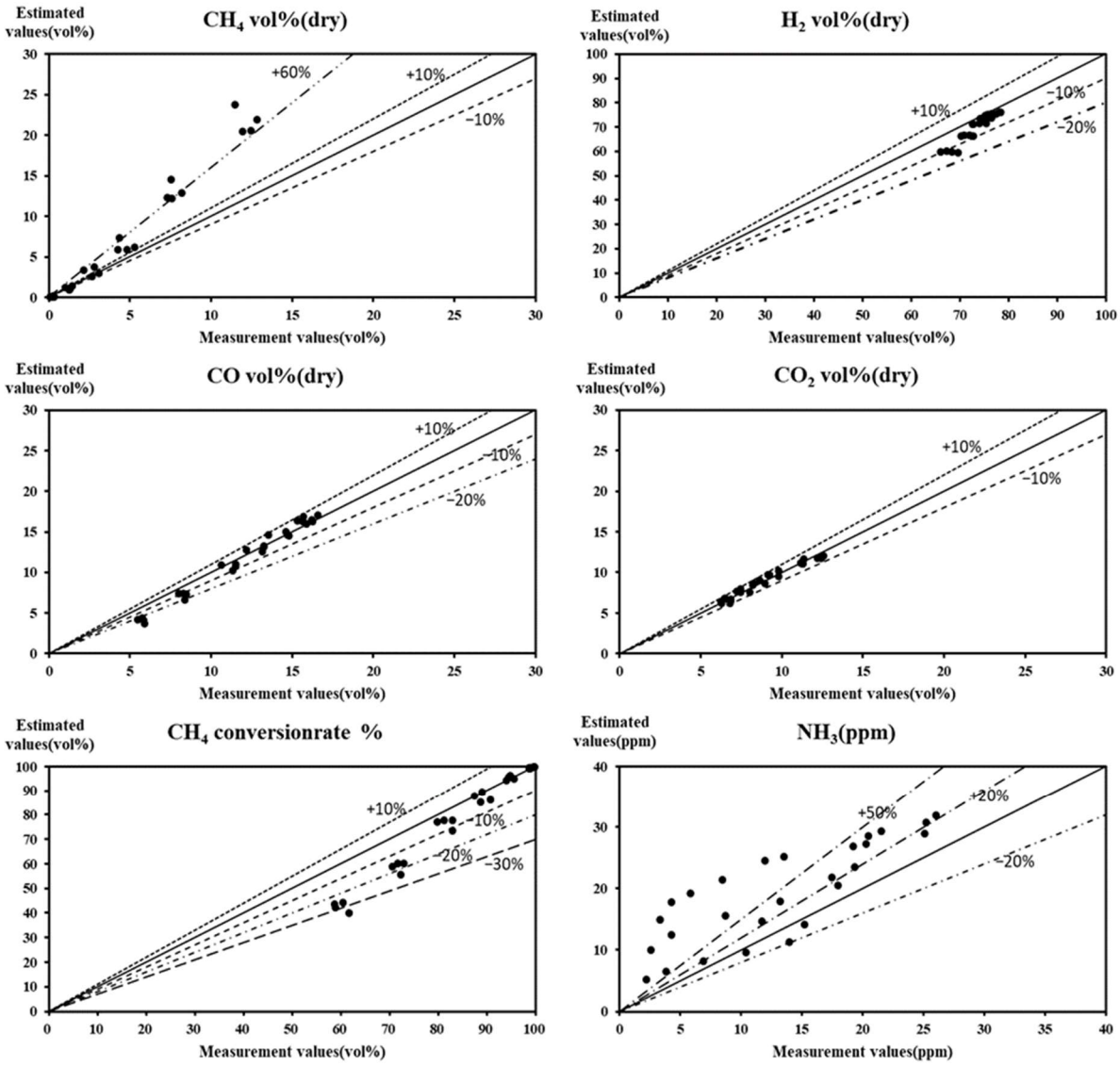

Figure 4. NH_3 power-law model reactor exit composition calculations vs. experimental results. Black circle (•) indicate measured and calculated values under the same experimental conditions.

Table 11. Optimized parameters for the Langmuir–Hinshelwood-based kinetic model for ammonia formation (adsorption term fixed).

NH_3 Kinetics Parameters					
A_{n2} (mol/g.h.bar)	E_{n2} (kJ/mol)	A_{co} (bar^{-1})	ΔH_{co} (kJ/mol)	A_H ($bar^{-1/2}$)	ΔH_H (kJ/mol)
4.7953	8.2667×10^1	9.0900×10^{-5}	-9.5343×10^1	6.7500×10^{-6}	-7.6548×10^1

Table 12. Optimized parameters for the Langmuir–Hinshelwood-based model (CO-adsorption term fixed).

NH_3 Kinetics Parameters			
A_{n2} (mol/g.h.bar)	E_{n2} (kJ/mol)	A_{co} (bar^{-1})	ΔH_{co} (kJ/mol)
5.3597	8.7339×10^1	9.0900×10^{-5}	-9.5343×10^1

Table 13. Optimized parameters for the Langmuir–Hinshelwood-based model (H adsorption term fixed).

NH_3 Kinetics Parameters			
A_{n2} (mol/g.h.bar)	E_{n2} (kJ/mol)	A_H ($bar^{-1/2}$)	ΔH_H (kJ/mol)
4.9920	8.0381×10^{1}	6.7500×10^{-6}	-7.6548×10^{1}

Table 14. Average errors for the three Langmuir–Hinshelwood-based models.

NH_3 Average Error			
Adsorption Term	CO and H	CO	H
Error (%)	57.05%	68.14%	54.02%

The ammonia production measured in experiment 2 and the ammonia production calculated from the 1D simple SR-reactor numerical model are plotted. The simplified power-law model is explained in Equations (14)–(16).

For the 1D simple SR-reactor numerical model, the ammonia-production-reaction rate was calculated using a power-law model that simplifies the Temkin–Pyzhev equation by assuming that the reactant gas in the SR reactor contains a relative excess of hydrogen compared to nitrogen. The optimized kinetics parameters of the power-law model of the ammonia-formation rate are shown in Table 9. Using the parameters in Table 9, the ammonia-production rate was applied to a simple SR-reactor simulation to calculate the outlet composition and ammonia production of the SR reactor. A graph comparing the values calculated from the simple SR-reactor simulation and the outlet composition measured in experiment set 2 is shown in Figure 4.

In the high conversion region, the experimental and calculated values are in good agreement within 10% error for the outlet-flow-concentration prediction and the methane-conversion rate. In the low-conversion region, the calculated value tends to be lower than the measured value, so the average error for methane concentration is 44%. In the case of carbon monoxide and carbon dioxide as shown in Figure 4, the difference between the experimental value and the measured value is within the error range of 10~20%. The ammonia-concentration-prediction results of the outlet flow show an error of about 20% at the higher-ammonia-concentration region (above 15 ppm), but at the lower-concentration regions (below 15 ppm) the scatter increases, and the prediction shows higher calculated concentrations. The average error of the predicted value of ammonia concentration is 88% (Table 10).

The results of optimizing all parameters of the Langmuir–Hinshelwood-based-model kinetics derived by applying the assumption that CO and H occupy the vacant active sites during the SR reaction to the ammonia-formation rate are shown in Table 11 (Equations (18) and (21)–(23)).

In the Langmuir–Hinshelwood-based model of ammonia formation, which considers the active site occupancy of CO and H, the parameters of the adsorption of CO and H in the denominator are fixed to the same values as the parameter values of the adsorption terms in the kinetic model of the SR reaction, since the reactant consumption of the ammonia reaction is very much smaller and the same catalyst is used for both cases.

A graph comparing the ammonia composition at the reactor outlet calculated by applying the Langmuir–Hinshelwood-based model in a 1D simple SR-reactor simulation using the parameters in Table 11 and the measured ammonia composition at the reactor outlet in experiment set 2 is shown in Figure 5.

A comparison between the calculated concentration of ammonia and the measured concentration is shown in Figure 5. The x-axis of the graph is the measured ammonia concentration in experiment set 2, and the y-axis is the concentration calculated via the Langmuir–Hinshelwood-based model with optimized parameters that considers the ad-

sorption of CO and H. The results in Figure 5 show that the model under-predicts the ammonia concentration.

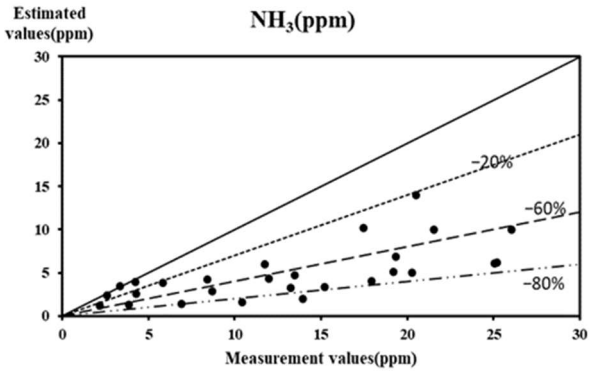

Figure 5. NH_3 calculation versus experiment result (The Langmuir–Hinshelwood-based model). Black circle (●) indicate measured and calculated values under the same experimental conditions.

The Langmuir–Hinshelwood-based model of the ammonia-formation reaction, derived by applying the assumption that carbon monoxide formed via the SR reaction has a large effect on occupying the vacant active site of the catalyst during the ammonia-formation reaction, was applied to the SR-reactor numerical model to estimate the ammonia-formation-rate parameters, and the results are shown in Table 12. The parameters of the carbon-monoxide-adsorption term in the denominator of this model are the values of the carbon-monoxide-adsorption term from the SR kinetics in Table 5.

A comparison between the calculated ammonia concentration at the outlet of the SR reactor and the measured concentration at the outlet flow in experiment set 2 is shown in Figure 6.

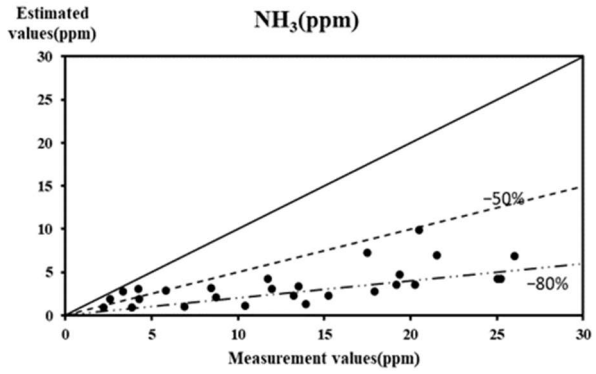

Figure 6. NH_3 calculation versus experiment result (CO-adsorption term only). Black circle (●) indicate measured and calculated values under the same experimental conditions.

The *x*-axis of the graph is the measured concentration of NH_3 of experiment set 2, and the *y*-axis is the concentration of the ammonia calculated by applying the parameter estimates of the Langmuir–Hinshelwood-based model that considers the adsorption of CO. The results in Figure 6 show that calculated concentrations are smaller than measured concentrations. Both the Langmuir–Hinshelwood-based model for the ammonia-formation reaction in the SR reactor (shown in Section 4 Experiments), assuming CO and H as adsorption terms, and the Langmuir–Hinshelwood-based model assuming only CO as adsorption term, show that the calculated ammonia concentrations in the flow are lower than the experimentally measured concentrations. Thus the parameters of the ammonia formation were estimated by applying the Langmuir–Hinshelwood model where only H is considered as the adsorption term. The Langmuir–Hinshelwood-based model of the ammonia-formation reaction, derived by applying the assumption that hydrogen has a large effect on occupying the vacant active sites of the catalyst during the ammonia-formation

reaction, is listed in the Equations (18), (22) and (25). The parameters of the hydrogen term in the denominator of this model are fixed using the values of the hydrogen term in the SR kinetics in Table 5, and the results of the optimized parameters of the ammonia-formation rate are summarized in Table 13.

The comparison between calculated ammonia production at the outlet of the SR reactor and measured concentrations in experiment set 2 is shown in Figure 7.

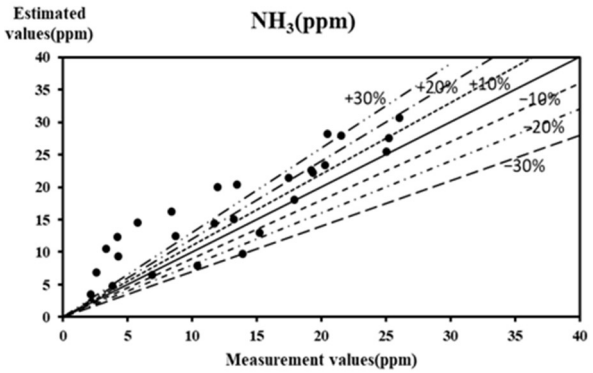

Figure 7. NH_3 calculation versus experiment (H adsorption term only). Black circle (•) indicate measured and calculated values under the same experimental conditions.

The *x*-axis of the graph is the measured ammonia concentrations in experiment set 2, and the *y*-axis is calculated ammonia-formation concentrations in a 1D simple SR-reactor numerical model via the Langmuir–Hinshelwood-based model, which takes into account the adsorption of H. The results in Figure 7 show that the slope of the trend line is close to 1, indicating that the trend of the ammonia-formation rate from the numerical model and those from the experiment are the same. Compared to the estimation results of the previous three models as shown in Table 14, the Langmuir–Hinshelwood-based model considering hydrogen adsorption predict the ammonia-formation rate the best since it follows the trend of experimental data.

4. Experiments

Two sets of RUA (Ru/Al_2O_3)-catalyzed methane steam-reforming reaction experiments were conducted in a tube-type reactor. Experimental set 1 was conducted to optimize the kinetic parameters of the steam-reforming (SR) reaction and water–gas-shift (WGS) reaction (side reaction) with Ru catalyst in an SR reactor, and experimental set 2 was conducted to measure the ammonia-formation rate in the steam-reforming reaction as a side reaction with N_2 containing process natural gas (PNG). Information about RUA (Ru/Al_2O_3) catalysts used for both sets of experiments is shown in Table 15. An electric furnace was installed in an SR reactor to supply the heat needed for the reaction. The reactor-outlet-gas composition was measured via a gas analyzer (NOVA prime-MRU model, Neckarsulm, Germany).

Table 15. Catalyst information.

Catalyst	Size	Shape	Content	Support
Ru	3 mm	Sphere	2 (wt%)	α-Al_2O_3

The schematic diagram of the experimental setup is in Figure 8. A mass flow controller (MFC) made by Linetech was used for the flow control of the feed gas and a metering pump was used for the supply of H_2O. The reactor was loaded with 109.56 g of Ru catalyst for SR reaction.

In experimental set 1, to estimate the kinetics parameters of SR and WGS reactions, the S/C ratio was kept at 2.5. The experimental conditions are summarized in Table 16.

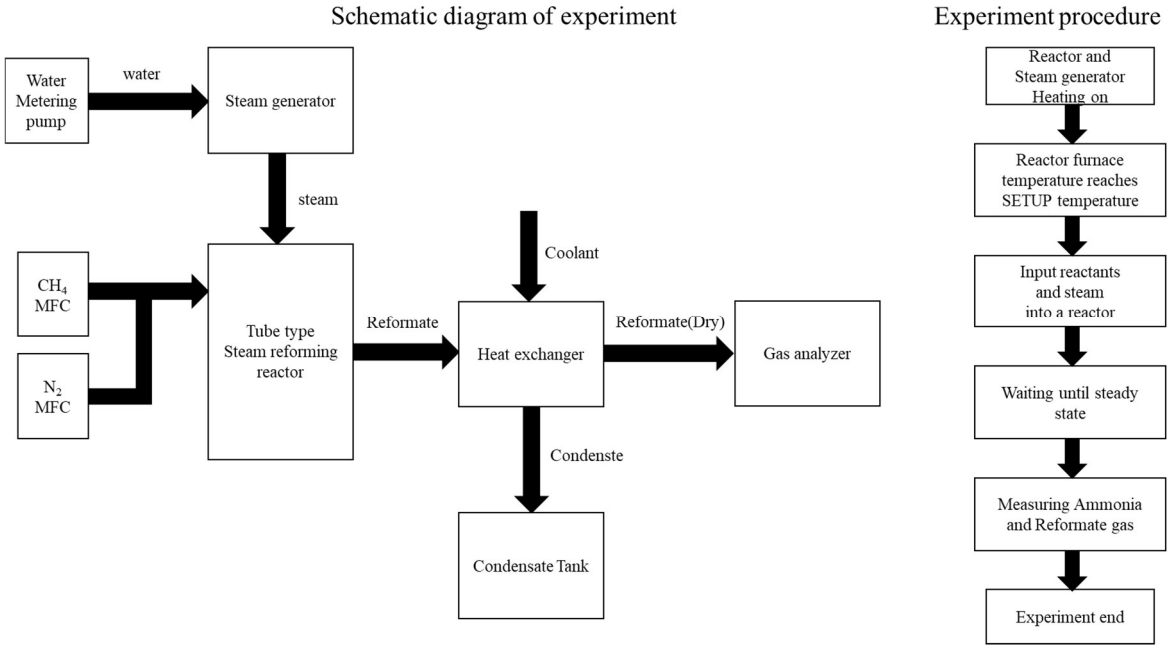

Figure 8. Schematic diagram of experiment and procedure.

Table 16. Experiment 1 conditions for SR and WGS kinetic parameters estimation.

Experimental Conditions			
Experiment	**Furnace Temperature (°C)**	**F_{CH4_i} (mol/h)**	**F_{H2O_i} (mol/h)**
1	500	2.6771	6.69
2	500	2.9449	7.36
3	520	2.6771	6.69
4	520	3.4803	8.70
5	550	2.6771	6.69
6	550	3.4803	8.70
7	580	2.6771	6.69
8	580	3.7480	9.37

The reactor surface temperatures were measured by attaching six k-type thermocouples to the reactor surface as shown in Figure 9.

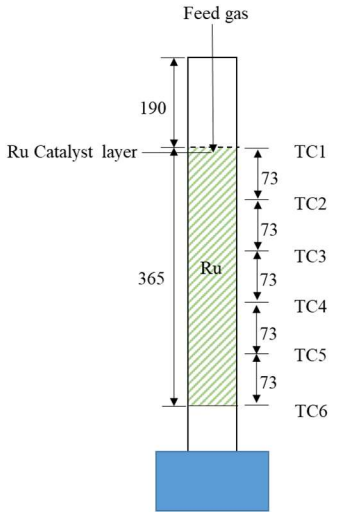

Figure 9. Reactor T_C locations for SR and WGS kinetic experiments.

To measure the ammonia-formation rate in experiment set 2, the flow rate of CH_4 supplied to the reactor was 2.3~2.8 mol/h and mixed with N_2 at concentrations of 3, 6, 9, and 10% as shown in Table 17. During experiments, the S/C ratio was fixed at 2.5.

Table 17. Experimental conditions for NH_3-formation experiment set 2.

Experimental Conditions for NH_3 Formation				
Experiment No.	**Furnace Temperature (°C)**	**F_{CH4_i} (mol/h)**	**F_{H2O_i} (mol/h)**	**N_2/CH_4**
1	520	2.8295	7.0738	0.03
2	550	2.7278	6.8195	0.03
3	580	2.6314	6.5785	0.03
4	600	2.5725	6.4313	0.03
5	620	2.5136	6.2840	0.03
6	650	2.4333	6.0833	0.03
7	680	2.3557	5.8893	0.03
8	520	2.8054	7.0135	0.06
9	550	2.7037	6.7593	0.06
10	580	2.6100	6.5250	0.06
11	600	2.5484	6.3710	0.06
12	620	2.4922	6.2305	0.06
13	650	2.4119	6.0298	0.06
14	670	2.3610	5.9025	0.06
15	520	2.7840	6.9600	0.09
16	550	2.6823	6.7058	0.09
17	580	2.5859	6.4648	0.09
18	600	2.5297	6.3243	0.09
19	620	2.4708	6.1770	0.09
20	650	2.3905	5.9763	0.09
21	670	2.3396	5.8490	0.09
22	520	2.6769	6.6923	0.10
23	550	2.6769	6.6923	0.10
24	580	2.6769	6.6923	0.10
25	600	2.6769	6.6923	0.10
26	620	2.6769	6.6923	0.10
27	650	2.6769	6.6923	0.10

To measure the reactor surface temperatures, three k-type thermocouples were installed on the surface of the catalyst layer as shown in Figure 10.

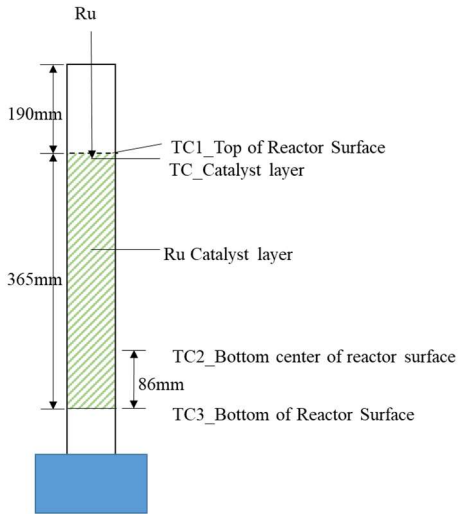

Figure 10. Installed positions of thermocouples in experiment set 2.

To measure the ammonia-formation rate, the outlet gas of the SR reactor was cooled and condensed, and condensate was collected. Additionally, the flow rate of heat-exchanger outlet gas was measured to calculate the ammonia composition of the outlet gas. The total amount of ammonia produced over time was measured by the summation of the amount of ammonia dissolved in a condensate over time and the amount of ammonia in the outlet gas over time. The amount of ammonia dissolved in the condensate was quantitatively measured via the colorimetric method using a Compact Ammonia Duo coloricmeter with Palintest. The composition of each component in the outlet gas was measured via a gas analyzer (NOVA prime-MRU). The molarity of the SR reactor outlet gas was calculated with the measured outlet-gas composition and the measured outlet gas flow rate. Using the exit gas molarity and the amount of ammonia in the condensate, the ammonia flow rate produced by the SR reactor was calculated.

5. Conclusions

Ru catalyst causes N_2 to react with H_2 to form ammonia at steam-reforming conditions and if supplied to the PEMFC, produced ammonia would seriously damage the PEMFC fuel cell. The European sort contains 1–5% or more N_2 in natural gas. Thus, to use a fuel-processing system for hydrogen production supplied to PEMFC in Europe, it is essential to investigate the ammonia concentration in a fuel-processing product gas to prevent ammonia formation. The Ru/Al_2O_3-catalyzed-SR-reaction and ammonia-formation-reaction experiments were conducted in a tube-type reactor and then numerically modeled by combining a simple 1D-reactor-simulation model with a kinetic model. The numerical modeling used a power-law model that simplifies the traditional ammonia-generation kinetics by Temkin–Pyzhev with the assumption that it reacts in an excess amount of hydrogen, and a Langmuir–Hinshelwood-based model with the assumptions that methane dissociative adsorption is the rate-limiting step and adsorbed CO and H cover the active sites of the catalyst affecting the overall activity. To optimize the kinetic parameters for each model, the multi-objective optimization method was used. The results of the numerical model showed that the model with the assumption that H_2 adsorbs and partially covers the active sites of the catalyst gave a better correlation with the experimental data. The new model would predict the ammonia concentration in the outlet flow of the fuel-processing system under various conditions and this information would be used to find operating conditions for the reformer to reduce the ammonia formation.

Author Contributions: Conceptualization, C.K. and S.L.; Formal analysis, C.K. and S.L.; Investigation, C.K. and J.L.; Writing—original draft, C.K.; Writing—review & editing, S.L.; Supervision, S.L.; Project administration, S.L.; Funding acquisition, S.L. All authors have read and agreed to the published version of the manuscript.

Funding: This research was funded by the Korea Institute of Energy Technology Evaluation and Planning (KETEP), grant number 20183010032400 and 20203040030110.

Data Availability Statement: New own data is contained within the article. Other data have been cited.

Acknowledgments: The authors are thankful to the Korea Institute of Energy Technology Evaluation and Planning (KETEP) for the support grant funded by the Korea government Ministry of Trade, Industry and Energy under the project titled: "Development on localization technologies of export-purposed stationary fuel cell systems", numbered: 20183010032400 and project titled: "Fuel cell safety demonstration linked to hydrogen extractor for public buildings", numbered: 20203040030110.

Conflicts of Interest: The authors declare no conflict of interest.

References

1. Mueller, F.; Jabbari, F.; Brouwer, J. On the intrinsic transient capability and limitations of solid oxide fuel cell systems. *J. Power Sources* **2009**, *187*, 452–460. [CrossRef]
2. Ye, M.; Wang, X.; Xu, Y. Parameter identification for proton exchange membrane fuel cell model using particle swarm optimization. *Int. J. Hydrogen Energy* **2009**, *34*, 981–989. [CrossRef]

3. Deng, Z.; Cao, H.; Li, X.; Jiang, J.; Yang, J.; Qin, Y. Generalized predictive control for fractional order dynamic model of solid oxide fuel cell output power. *J. Power Sources* **2010**, *195*, 8097–8103. [CrossRef]
4. Larminie, J.; Dicks, A. *Fuel Cell Systems Explained*; John Wiley & Sons Ltd.: Chichester, UK, 2003; Volume 2.
5. Suiso. *Nenryou Denchi Handbook Henshu Iinlcai. Suiso. Nenryou Denchi Handbook*; Ohmsha: Tokyo, Japan, 2006.
6. Hashimasa, Y.; Matsuda, Y.; Imamura, D.; Akai, M. PEFC Power Generation Performance Degradation by Hydrogen Sulfide and Ammonia—Effects of Lowering Platinum Loading—. *Electrochemistry* **2011**, *79*, 343–345. [CrossRef]
7. Watanabe, F.; Kaburaki, I.; Shimoda, N.; Satokawa, S. Influence of nitrogen impurity for steam methane reforming over noble metal catalysts. *Fuel Process. Technol.* **2016**, *152*, 15–21. [CrossRef]
8. Jakobsen, J.G.; Jørgensen, T.L.; Chorkendorff, I.; Sehested, J. Steam and CO_2 reforming of methane over a Ru/ZrO_2 catalyst. *Appl. Catal. A Gen.* **2010**, *377*, 158–166. [CrossRef]
9. Jakobsen, J.G.; Jakobsen, M.; Chorkendorff, I.; Sehested, J. Methane Steam Reforming Kinetics for a Rhodium-Based Catalyst. *Catal. Lett.* **2010**, *140*, 90–97. [CrossRef]
10. Jones, G.; Jakobsen, J.G.; Shim, S.S.; Kleis, J.; Andersson, M.P.; Rossmeisl, J.; Abild-Pedersen, F.; Bligaard, T.; Helveg, S.; Hinnemann, B.; et al. First principles calculations and experimental insight into methane steam reforming over transition metal catalysts. *J. Catal.* **2008**, *259*, 147–160. [CrossRef]
11. Mozdzierz, M.; Brus, G.; Sciazko, A.; Komatsu, Y.; Kimijima, S.; Szmyd, J.S. Towards a Thermal Optimization of a Methane/Steam Reforming Reactor. *Flow Turbul. Combust* **2016**, *97*, 171–189. [CrossRef]
12. Na, W.; Gou, B. The efficient and economic design of PEM fuel cell systems by multi-objective optimization. *J. Power Sources* **2007**, *166*, 411–418. [CrossRef]
13. Boudart, M. Kinetics and Mechanism of Ammonia Synthesis. *Catal. Rev.* **1981**, *23*, 1–15. [CrossRef]
14. Aparicio, L.M.; Dumesic, J.A. Ammonia synthesis kinetics: Surface chemistry, rate expressions, and kinetic analysis. *Top. Catal.* **1994**, *1*, 233–252. [CrossRef]
15. Rossetti, I.; Pernicone, N.; Ferrero, F.; Forni, L. Kinetic Study of Ammonia Synthesis on a Promoted Ru/C Catalyst. *Ind. Eng. Chem. Res.* **2006**, *45*, 4150–4155. [CrossRef]
16. Ozaki, A.; Taylor, H.S.; Boudart, M. Kinetics and mechanism of the ammonia synthesis. *Proc. R. Soc. Lond. A* **1960**, *258*, 47–62. [CrossRef]
17. Temkin, M.; Pyzhev, V. Kinetics of the synthesis of ammonia on promoted iron catalysts. *Acta Physicochim.* **1940**, *12*, 217–222.
18. Zhu, J.; Cui, X.; Araya, S.S. Comparison between 1D and 2D numerical models of a multi-tubular packed-bed reactor for methanol steam reforming. *Int. J. Hydrogen Energy* **2022**, *47*, 22704–22719. [CrossRef]
19. Sun, J.; DesJardins, J.; Buglass, J.; Liu, K. Noble metal water gas shift catalysis: Kinetics study and reactor design. *Int. J. Hydrogen Energy* **2005**, *30*, 1259–1264. [CrossRef]
20. Rosowski, F.; Hornung, A.; Hinrichsen, O.; Herein, D.; Muhler, M.; Ertl, G. Ruthenium catalysts for ammonia synthesis at high pressures: Preparation, characterization, and power-law kinetics. *Appl. Catal. A Gen.* **1997**, *151*, 443–460. [CrossRef]

Disclaimer/Publisher's Note: The statements, opinions and data contained in all publications are solely those of the individual author(s) and contributor(s) and not of MDPI and/or the editor(s). MDPI and/or the editor(s) disclaim responsibility for any injury to people or property resulting from any ideas, methods, instructions or products referred to in the content.